Microstructure of Cell Wall-Associated Melanin in the Human Pathogenic Fungus *Cryptococcus neoformans*†

Helene C. Eisenman,‡ Joshua D. Nosanchuk,‡ J. Beau W. Webber,§ Ray J. Emerson,|| Terri A. Camesano,|| and Arturo Casadevall*,‡,⊥

Division of Infectious Diseases of the Department of Medicine and Department of Microbiology and Immunology, Albert Einstein College of Medicine, 1300 Morris Park Avenue, Bronx, New York 10461, School of Physical Sciences, University of Kent, Canterbury, Kent CT2 7NR, U.K., and Department of Chemical Engineering, Worcester Polytechnic Institute, 100 Institute Road, Worcester, Massachusetts 01609

Received October 24, 2004; Revised Manuscript Received December 17, 2004

ABSTRACT: Melanin is a virulence factor for many pathogenic fungal species, including *Cryptococcus neoformans.* Melanin is deposited in the cell wall, and melanin isolated from this fungus retains the shape of the cells, resulting in hollow spheres called "ghosts". In this study, atomic force, scanning electron, and transmission electron microscopy revealed that melanin ghosts are covered with roughly spherical granular particles approximately 40−130 nm in diameter, and that the melanin is arranged in multiple concentric layers. Nuclear magnetic resonance cryoporometry indicated melanin ghosts contain pores with diameters between 1 and 4 nm, in addition to a small number of pores with diameters near 30 nm. Binding of the antibodies to melanin reduced the apparent measured volume of these pores, suggesting a mechanism for their antifungal effect. We propose a model of cryptococcal melanin structure whereby the melanin granules are held together in layers. This structural model has implications for cell division, cell wall remodeling, and antifungal drug discovery.

Cryptococcus neoformans is a frequent cause of life-threatening fungal disease in immunocompromised patients (*1*). This yeastlike fungus is remarkable in being an encapsulated eukaryotic human pathogen, of which there are few known examples (*2*, *3*). Cryptococcal infections are presumably contracted by inhalation of infectious particles that reside in the environment. In the majority of healthy hosts, the infection is contained in the lungs. However, in individuals with impaired immunity, dissemination can occur, frequently to the central nervous system. Like many fungal infections, cryptococcosis is notoriously difficult to treat. Therefore, it is important to understand factors that contribute to virulence for the development of more effective therapies.

One key factor that contributes to the pathogenesis of *C. neoformans*, as well as other fungi, is melanin (*4*, *5*). Comparison of melanized and nonmelanized strains of *C. neoformans* in animal models of infection reveals that nonmelanotic *C. neoformans* strains are less virulent, thereby establishing the importance of melanin to virulence (*6*, *7*). Melanin has been found to affect the immune system. Fungal melanins are immunogenic and can elicit antibodies that inhibit fungal growth (*8*−*11*). Furthermore, melanization is associated with decreased levels of inflammatory cytokines in animal models of infection (*12*, *13*). Melanization decreases the rate of phagocytosis and killing of *C. neoformans* by macrophages (*14*) and increases resistance to microbicidal peptides in vitro (*15*). Together, these studies suggest that melanin in *C. neoformans* increases virulence by reducing the vulnerability of fungal cells to host defense mechanisms and interfering with the development of effective immune responses. In addition to increasing resistance of *C. neoformans* to immune defenses, melanin also reduces the efficacy of certain antifungal drugs (*16*−*18*). Thus, melanization has clinical implications for *C. neoformans* infections in terms of both the immune response and the ability to use and develop newer antifungal drugs.

Melanization occurs in the environment (*19*) and is important for survival. Melanin protects *C. neoformans* from various environmental conditions, such as the presence of toxins, extreme temperatures, and ultraviolet radiation (*20*−*23*). Additionally, melanin provides defense from environmental predation by microorganisms such as the nematode, *Caenorhabditis elegans*, and the amoeba *Acanthamoeba castellani* (*24*, *25*). Thus, melanin has a protective role in *C. neoformans* both in the host and in the environment.

Melanin in *C. neoformans* is found in the cell wall (*14*, *26*). Synthesis of melanin is dependent on a laccase enzyme and the presence of exogenous substrates, such as L-3,4-

† This work was supported by National Institutes of Health Grants AI33774, AI13342, AI052733, HL59842 (A.C.), and T32CA09173 (H.C.E.).

* To whom correspondence should be addressed: Albert Einstein College of Medicine, 1300 Morris Park Ave., Golding 701, Bronx, NY 10461. E-mail: casadeva@aecom.yu.edu. Telephone: (718) 430-3665. Fax: (718) 430-8701.

‡ Division of Infectious Diseases of the Department of Medicine, Albert Einstein College of Medicine.

§ University of Kent.

|| Worcester Polytechnic Institute.

⊥ Department of Microbiology and Immunology, Albert Einstein College of Medicine.

10.1021/bi047731m CCC: $30.25
Published on Web 02/15/2005

dihydroxyphenylalanine (L-dopa)[1] and epinephrine (*27*, *28*). Although the details of melanin structure are largely unknown, it is believed to be a cross-linked polymer of phenol and indole subunits (*29*, *30*). Melanin is a highly stable compound and can be isolated from cells by harsh chemical treatments that degrade other cellular components such as the cell wall, lipids, and proteins. Such treatment produces hollow melanin shells called "ghosts" that retain the spherical shape of the cells (*31*).

The presence of melanin in *C. neoformans* leads to challenges in the treatment of this disease. The effects of melanization on the basic biological mechanisms of the organism, including how nutrients are transported across the melanin layer and how cells bud through melanin, are not understood. To formulate a model of how these processes occur, it is necessary to determine the structure of the melanin layer. Unfortunately, melanins are poorly characterized because they are insoluble amorphous materials not suitable for crystallization or solution studies. To gain structural insights, complementary techniques were applied to the study of melanin. These included atomic force microscopy (AFM) and scanning electron microscopy (ScEM) for imaging of the melanin surface, transmission electron microscopy (TEM) for cross-sectional analysis of melanin ghosts, and nuclear magnetic resonance (NMR) cryoporometry for determination of the porosity of melanin. On the basis of results from these studies, we propose a model of melanin structure composed of multiple layers of densely packed granules whereby pores and channels are formed in the spaces between melanin particles. This model has implications for the mechanism of budding of melanized cells and the antifungal action of melanin-binding antibodies.

EXPERIMENTAL PROCEDURES

C. neoformans Strains and Media. *C. neoformans* serotype D strain 24067 was obtained from the American Type Culture Collection (Manassas, VA). *C. neoformans* serotype D strain Cap67, containing a mutation in the *CAP59* gene, was generously provided by J. Kwon-Chung (*32*). The cells were grown in defined chemical media [minimal medium, 15 mM dextrose, 10 mM $MgSO_4$, 29.4 mM KH_2PO_4, 13 mM glycine, and 3 μM thiamine (pH 5.5)] with 1 mM L-dopa, epinephrine, or dopamine (Sigma-Aldrich, St. Louis, MO). Cultures (500 mL) were incubated in the dark at 30 °C in 1 L Erlenmeyer flasks in a rotary shaker at 150 rpm for the indicated times.

Antibodies. Melanin-binding antibodies and their use have been described previously (*33*). Briefly, mice were immunized with L-dopa melanin ghosts. Spleen cells from mice producing antibodies to melanin were fused to myeloma cells to generate hybridomas for the production of monoclonal antibodies to melanin. MAb 5C11, recognizing mycobacterial lipoarabinomannan, was used as a control (*34*).

Preparation of Melanin Ghosts from Cells Grown in Vitro. *C. neoformans* strain 24067 was cultured in defined chemical media with 1 mM L-dopa, epinephrine, or dopamine at 30 °C for the indicated times. Melanin ghosts were isolated by enzymatic digestion of the cell wall, proteolysis, chloroform extraction, and boiling in concentrated HCl as described previously (*35*).

In Vivo Melanin Ghost Isolation. BALB/c mice were infected by intravenous injection in the tail vein with 5×10^5 *C. neoformans* strain 24067 cells. After 21 days, infected mice were sacrificed and melanin ghosts were isolated from infected tissues. The brains of infected mice were homogenized by mechanical grinding. Tissues were then treated with 1.0 mg/mL proteinase K (Boehringer Mannheim Co., Indianapolis, IN) at 65 °C for 4 h, incubated in 4.0 M guanidine thiocyanate for at least 2 h at room temperature with frequent vortexing, and then boiled in 6.0 M HCl for 1 h. The resulting material was washed three times with phosphate-buffered saline (PBS) [8 g/L NaCl, 0.2 g/L KCl, 0.2 g/L KH_2PO_4, and 1.2 g/L Na_2HPO_4 (pH 7.4)] and prepared for ScEM as described below.

Nuclear Magnetic Resonance Cryoporometry. Melanin ghosts were prepared from cells grown for 4, 7, or 10 days in the presence of a substrate (i.e., 1 mM L-dopa or epinephrine). For the melanin antibody studies, melanin ghosts were isolated from cells grown for 10 days in the presence of L-dopa. Ghosts were incubated with SuperBlock (Pierce, Rockford, IL) to prevent nonspecific binding and then incubated with a melanin-binding or control antibody at a concentration of 10 μg/mL prior to analysis. In addition, commercially prepared synthetic tyrosine melanin and *S. officinalis* melanin were analyzed (Sigma-Aldrich).

To analyze pore size by NMR cryoporometry, samples were frozen in water, and then slowly warmed at a rate of 0.2 °C/min. The change in melting point temperature was measured from the amplitude of the NMR signal from the protons in liquid water and used to determine porosity as a function of pore size using the Gibbs−Thomson equation (*36*−*38*).

The NMR cryoporometry measurements were made using a fast-recovery NMR relaxation spectrometer constructed at the University of Kent with gas-flow temperature control (liquid nitrogen to 500 K), which had been modified for highly precise (∼1 mK) relative temperature measurements (*37*). Samples were prepared in flame-sealed thin-walled silica tubes, with the measurement copper−constantan thermocouple soldered to a nonshorting copper foil around the sample, and the thermal EMF measured relative to a matched thermocouple in melting ice. NMR cryoporometry offers a number of advantages over the similar thermoporosimetry technique, including the ability to measure arbitrarily slowly and to improve both pore size resolution and the signal-to-noise ratio. These NMR cryoporometry measurements show a pore volume resolution of around 5 nL/Å.

Scanning Electron Microscopy. Melanin ghosts were isolated from *C. neoformans* cultures grown for 1, 2, or 3 weeks in the presence of 1 mM L-dopa or dopamine or from animals as described above. Following melanin ghost isolation, samples were fixed in 2.5% glutaraldehyde in 0.1 M cacodylate (pH 7.4). After being fixed, samples were dehydrated through a graded series of ethanol and critical point dried using liquid carbon dioxide in a Tousimis Samdri (Rockville, MD) 795 critical point drier. Samples were then sputter coated with gold−palladium (Desk-II; Denton Vacuum Inc., Cherry Hill, NJ). Imaging was performed with a JEOL (Peabody, MA) JSM-6400 scanning electron microscope

[1] Abbreviations: AFM, atomic force microscopy; L-dopa, L-3,4-dihydroxyphenylalanine; ScEM, scanning electron microscopy; TEM, transmission electron microscopy.

using an accelerating voltage of 10 kV. Images were acquired with analySIS (Soft Imaging System GmbH, Münster, Germany). For ScEM of acapsular cells, cultures (250 mL) of *C. neoformans* strain Cap67 were grown for 2 weeks in the dark in defined chemical media with or without 1 mM L-dopa in 500 mL Erlenmeyer flasks at 30 °C and 150 rpm. Cells were washed in PBS, fixed in 2.5% glutaraldehyde in 0.1 M cacodylate, dehydrated, and coated as described for melanin ghosts.

Transmission Electron Microscopy. Melanin ghosts were fixed in 2% glutaraldehyde in 0.1 M cacodylate at room temperature for 2 h, followed by overnight incubation in 4% formaldehyde, 1% glutaraldehyde, and 0.1% PBS. The samples were subjected to postfixation for 90 min in 2% osmium, serially dehydrated in ethanol, and embedded in Spurrs epoxy resin. Sections (70−80 nm thick) were cut on a Reichart Ultracut UCT and stained with 0.5% uranyl acetate and 0.5% lead citrate. Samples were viewed in a JEOL 1200EX transmission electron microscope at 80 kV.

Atomic Force Microscopy. For AFM studies, melanin ghosts were isolated from *C. neoformans* cultures grown for 7, 14, or 21 days in the presence of L-dopa. Glass slides for AFM were cleaned as described elsewhere (*39*). Melanin ghosts were immobilized on glass slides by mixing poly-L-lysine with a suspension of melanin ghosts [1 mL of a 10% (w/v) suspension added to 9 mL of ghost suspension containing between 5×10^8 and 1×10^9 ghosts/mL] and pipetting the mixture onto glass slides. AFM imaging was performed with a Digital Instruments Dimension 3100 (Veeco Instruments, Woodbury, NY) atomic force microscope with a Nanoscope IIIa controller. AFM was performed in air or water at room temperature under normal atmospheric pressure. Images were recorded in intermittent contact mode. For air experiments, cantilevers were TESPA (TappingMode Etched Silicon Probes with an Aluminum Backing-Layer) from Digital Instruments (Santa Barbara, CA), with a nominal spring constant of 100 N/m. In liquid, cantilevers were DNP-S (triangular silicon nitride probes with a gold backing layer), with a nominal spring constant of 0.13 N/m. All cantilevers were cleaned under UV light for 5 min prior to experiments to remove adsorbed water and hydrocarbons. The scan rate was 1.001 Hz. The number of samples was 256 lines/image and 256 pixels/line (65,536 total samples). The AFM laser diode wavelength and *Z*-direction step height were calibrated according to ref *40*. Imaging parameters were calibrated according to the manufacturer's specifications using a 180 nm pitted calibration standard. Data were analyzed using Nanoscope IIIa software (version 4.43 r8, Digital Instruments) and Scanning Probe Imaging Processor (SPIP) software (Image Metrology). To determine granule size diameter, the edges of the granules were marked on the sectional analysis of the image and corresponding coordinates used to measure granules.

RESULTS

Overall Structure of Melanin Ghosts. Melanin ghosts were isolated from melanized *C. neoformans* cells grown in liquid media containing L-dopa for 1, 2, or 3 weeks. Samples were imaged by ScEM and AFM. The isolated ghosts retained the spherical shape of the cells (Figure 1). However, some collapsing of the melanin ghosts was observed by AFM (Figure 2D).

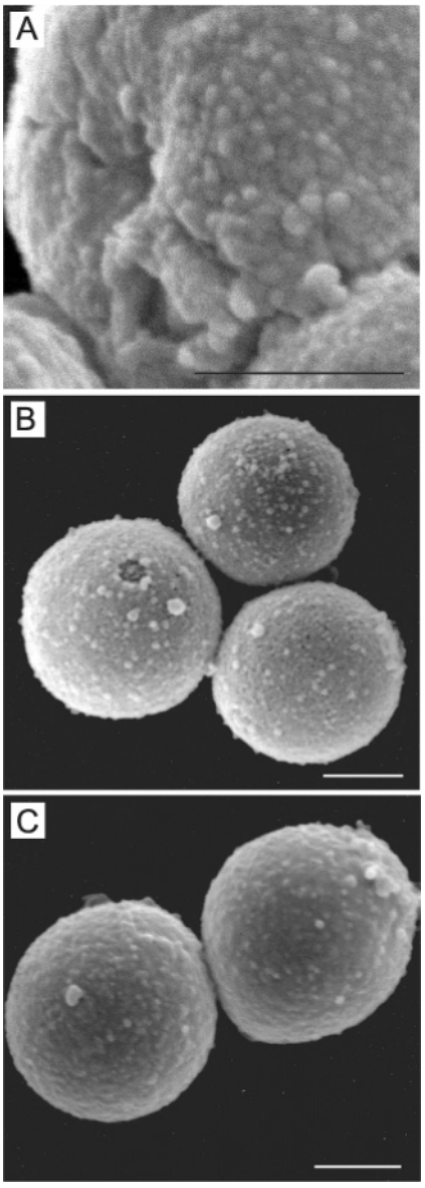

FIGURE 1: ScEM of granules on the surface of melanin ghosts. Scale bars are 1 μm. (A) High-resolution micrograph of melanin ghosts isolated from the 1 week culture of *C. neoformans* strain 24067 grown in the presence of L-dopa. (B) Melanin ghosts isolated from *C. neoformans* strain 24067 grown in the presence of dopamine for 10 days. (C) Melanin ghosts isolated from *C. neoformans*-infected mouse tissue harvested 21 days postinfection.

High-Resolution Surface Structure of Melanin. Two complementary imaging methods were used to visualize the surface of melanin ghosts isolated from *C. neoformans*: high-resolution ScEM and AFM (Figures 1 and 2, respectively). The most striking feature apparent from these images was the granular nature of the melanin surface (Figures 1A and 2B,C,E,F), a feature that was not described in previous studies (*31*, *33*). The ghost surface consisted of irregularly shaped granules with a geometry that approximated tightly packed spheres. Occasionally, ghosts were observed with the granules in an ordered linear arrangement (Figure 2E,F). The size of the granules was estimated by measurements from both the ScEM and AFM images (Figure 3). ScEM measurements revealed a diameter of 74 ± 13 nm for granules from 1 week melanin ghosts and 82 ± 21 nm for granules from 3 week ghosts, a small, but statistically significant difference

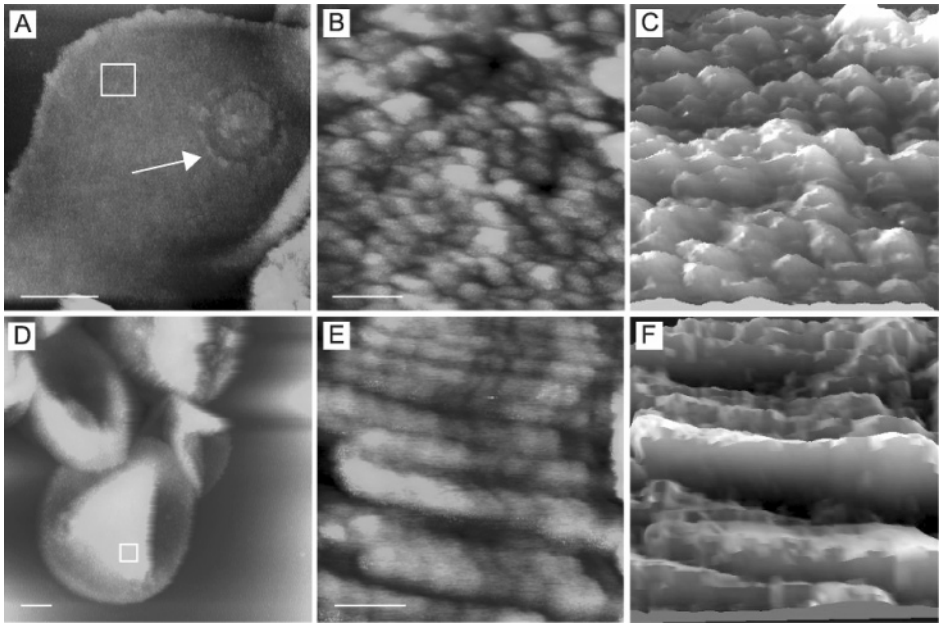

FIGURE 2: AFM surface analysis of melanin ghosts. Melanin ghosts were isolated from the 3 week culture of *C. neoformans* strain 24067 grown in the presence of L-dopa. AFM height images, showing the surface topology of melanin ghosts, are shown. (A) Overall shape of the melanin ghost imaged by AFM. The arrow points to a bud scar. The scale bar is 1 μm. (B) Close-up analysis of the surface indicated by the small rectangle in panel A. The scale bar is 100 nm. Images created using Nanoscope IIIa software (version 4.43 r8, Digital Instruments). (C) Three-dimensional rendering of the surface in panel B. This image was created with SPIP (Image Metrology). (D) Overall shape of melanin ghosts imaged by AFM. Ghosts are somewhat collapsed. The scale bar is 1 μm. (E) Close-up analysis of the surface indicated by the small rectangle in panel D. The scale bar is 100 nm. Images created using Nanoscope IIIa software (version 4.43 r8, Digital Instruments). (F) Three-dimensional rendering of the surface in panel E. This image was created with SPIP (Image Metrology).

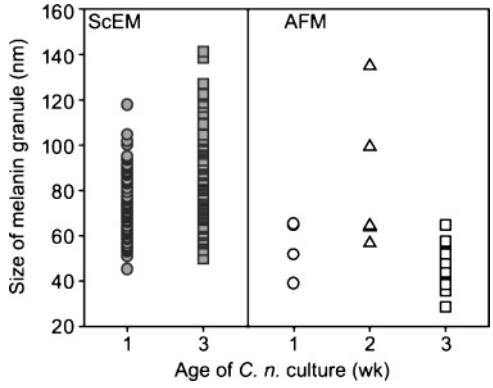

FIGURE 3: Analysis of melanin ghost granule size. The sizes of granules on the surface of 1, 2, and 3 week melanin ghosts were measured using ScEM and AFM images as described in Experimental Procedures (all data points are plotted). Data from ScEM are shown at the left and from AFM at the right: circles, 1 week samples; triangles, 2 week samples; and squares, 3 week samples.

in size ($P < 0.05$). In contrast, AFM measurements yielded an average particle diameter of 57 ± 12 nm for granules from 1 week ghosts, 81 ± 31 nm for granules from 2 week ghosts, and 49 ± 8 nm for granules from 3 week ghosts. For ScEM, 20 granules from each ghost were measured and 4−5 ghosts were analyzed. For AFM, 5−12 granules from each ghost were measured and 1−2 ghosts were analyzed.

Since the isolation of melanin ghosts requires harsh chemical treatments that could theoretically alter the melanin structure, we attempted to study the surface structure of melanin as it is found in intact cells by visualizing melanized and nonmelanized *C. neoformans* cells using ScEM (Figure 4) and AFM (data not shown). Since *C. neoformans* normally has a polysaccharide capsule that prevents surface inspection

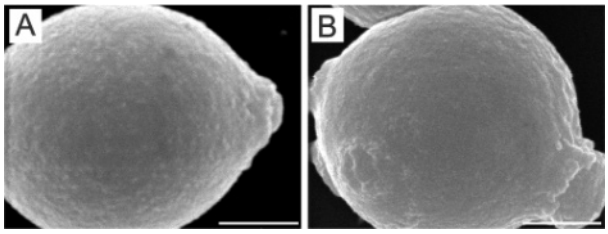

FIGURE 4: Melanin in *C. neoformans* cells is partially covered by portions of the cell wall. (A) ScEM images of melanized acapsular *C. neoformans*. Strain Cap67 was grown for 2 weeks in minimal media with L-dopa and then washed and fixed as described in Experimental Procedures. Scale bars are 1 μm. (B) Scanning EM images of nonmelanized acapsular *C. neoformans*. Strain Cap67 was grown for 2 weeks in minimal media and then washed and fixed as described in Experimental Procedures. Scale bars are 1 μm.

of the cell wall, an acapsular strain, Cap67, was used in this analysis (*32*). When viewed in the ScEM, the surfaces of both the melanized (Figure 4A) and nonmelanized (Figure 4B) cells were similar. Both appeared fairly smooth. This suggests that, in the cell, melanin was partially obscured by outer components of the cell wall. Consequently, it was not feasible to compare the surface structure of melanin ghosts to the surface of melanin in cells by these techniques.

Differences in the granularity of melanin were apparent around bud scars, which were manifested by significant increases in the granule size in areas near bud scars relative to other parts of the ghost surface (Figure 5A,B). Larger granules were observed near the bud scars. By AFM, the average particle size for the 3 week samples was 49 ± 8 nm far from the bud scars and 96 ± 29 nm near the bud scars ($P < 0.05$) (Figure 5C). Between 7 and 8 granules near bud scars from each of two different melanin ghosts were measured. AFM analysis of the average roughness revealed

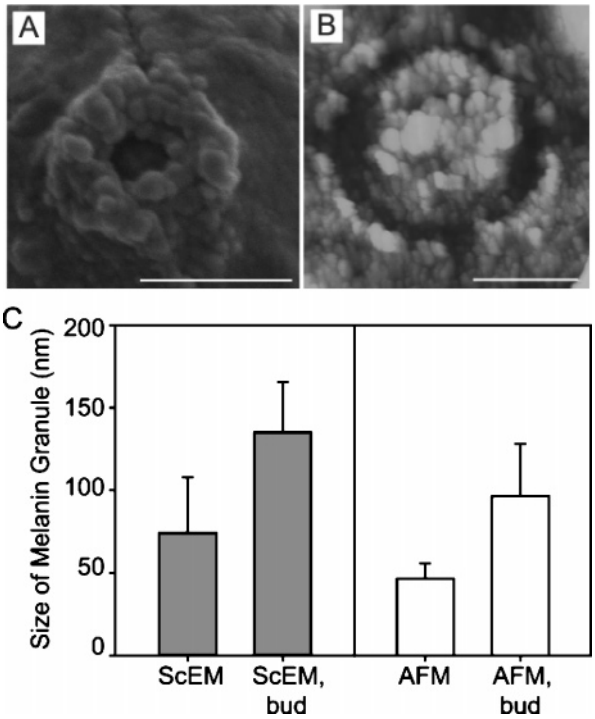

FIGURE 5: Melanin granules are larger near bud scars. (A) High-resolution ScEM of melanin ghosts isolated from the 1 week culture of *C. neoformans* strain 24067 grown in the presence of L-dopa. The scale bar is 1 μm. (B) AFM image of bud scar from melanin ghost isolated from the 3 week culture of *C. neoformans* strain 24067 grown in the presence of L-dopa. The scale bar is 0.5 μm. (C) Melanin granules were measured from ScEM and AFM images for areas near (ScEM, bud, and AFM, bud) or far (ScEM and AFM) from bud scars. Melanin ghosts isolated from 3 week *C. neoformans* cultures were analyzed. Graphs indicate the average size ± the standard deviation of melanin granules.

the same trend. The root-mean-square (rms) roughness of the ghost surface far away from the bud scar was 4.1 nm, whereas near the bud scar the roughness was 7.1 nm (data not shown).

$$\mathrm{rms} = \sqrt{\frac{\sum_{i=1}^{N}(Z_i - Z_{\mathrm{Ave}})^2}{N}}$$

where Z_{Ave} is the average height within the given area, Z_i is a discrete height within the area, and N is the number of points in the given area [*Scanning Probe Microscopy Training Notebook* (1998) pp 39−40, Digital Instruments, Veeco Metrology Group]. The same significant variation was apparent from ScEM of melanin ghosts. The average size of the granules near bud scars was 136 ± 8 nm for 3 week melanin ghosts, compared to 82 ± 21 nm for granules far from bud scars ($P < 0.05$) (Figure 5C). Between 12 and 19 granules near bud scars on each of three different melanin ghosts were measured. The difference in melanin granule size around bud scars may be due to alterations in the underlying cell wall architecture since similar structures were visible in acapsular cells, both melanized and nonmelanized (Figure 4 and data not shown).

Melanin Shell of C. neoformans Is Composed of Layers. Melanin ghosts were sectioned and visualized by TEM to gain insight into their cross-sectional structure. The TEM

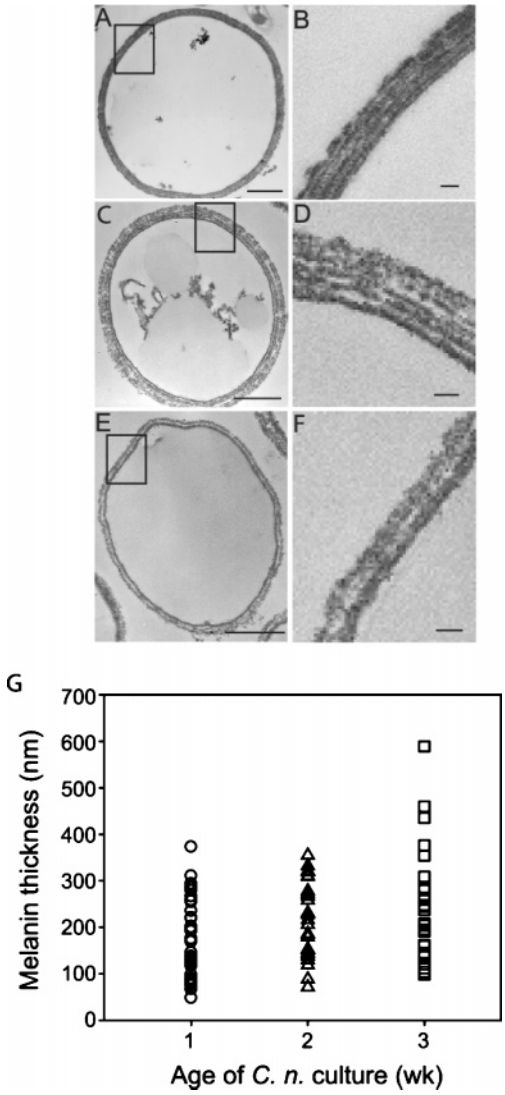

FIGURE 6: Melanin in *C. neoformans* is arranged in concentric layers. Transmission electron micrographs of three representative melanin ghosts. (A, C, and E) Cross section of melanin ghosts. Scale bars are 1 μm. (B, D, and F) Close-up of areas indicated by rectangles in panels A, C, and E, respectively. Scale bars are 100 nm. (G) The thickness of melanin shell was measured for 1, 2, and 3 week melanin ghosts, and all data points are plotted: circles, 1 week samples; triangles, 2 week samples; and squares, 3 week samples.

images revealed that the walls of the melanin ghosts were composed of two to five concentric layers (Figure 6B,D,F). Each layer was between 50 and 75 nm wide, and the average thickness of the melanin ghost wall was 200 ± 98 nm. The thickness of the melanin was measured for 1, 2, and 3 week samples, and average thicknesses were found to be 164 ± 82 ($n = 42$), 220 ± 81 ($n = 26$), and 241 ± 114 nm ($n = 30$), respectively (Figure 6G). One week melanin ghost shells were significantly different from 2 week ($P < 0.05$) and 3 week melanin ghosts ($P < 0.05$). Ghosts from budding cells showed that the melanin layer around the bud was thinner than that of the mother cell. An increase in thickness was observed for larger buds (Figure 7A−F). ScEM analysis of similar ghosts showed that the surface of the buds was often smoother than that of the mother cell (Figure 7G). This suggests that, in early buds, melanin deposition was not complete. Together, these results are consistent with an increase in melanin thickness over time.

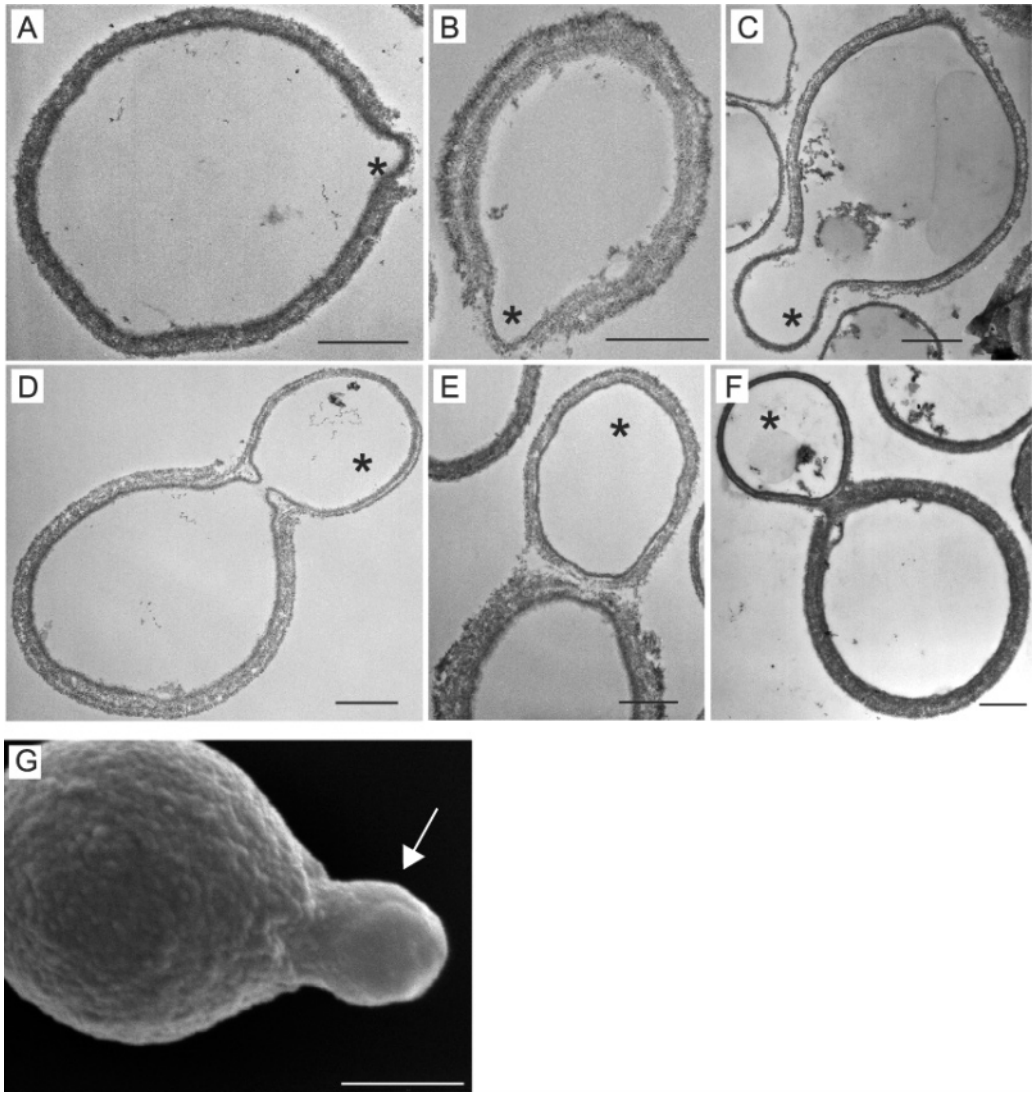

FIGURE 7: Melanin layer is thinner around buds. (A−F) Transmission electron micrographs of melanin ghosts made from cells in various stages of budding. An increase in melanin thickness with increasing bud size relative to the mother cell is apparent. Buds are marked with asterisks. Scale bars are 1 μm. (G) Scanning electron micrograph of a melanin ghost from a budding cell showing that melanin is smoother around the bud (white arrow).

Melanin Ghosts Have Pores. NMR cryoporometry was used to analyze the porosity of *C. neoformans* melanin. In this method, porosity was determined based on the change in melting point temperature of water in a pore versus a large volume (*36*, *38*). The melting point was measured by the amplitude of the NMR signal from the protons in liquid water. Cells were grown in liquid media containing L-dopa for 4, 7, or 10 days, and melanin ghosts were isolated. Samples were mechanically crushed with a mortar and pestle prior to analysis. By this technique, a pore was identified by the contained water melting at a lower temperature than the bulk water present around the melanin shells. The relative amplitudes of the pore water signal and the total water signal were recorded. Thus, the volume of this pore-contained water was directly measurable, as the total volume of the water in the sample was known from gravimetric measurements. Additional measurements were taken with commercially available melanin from *Sepia officinalis* ink sacs and synthetic tyrosine.

Of the *C. neoformans* melanin samples, day 4 melanin ghosts had the greatest porosity (a sharp peak of 41 μL Å^{-1} g^{-1} at 16.4 Å). Day 7 melanin ghosts showed a broad peak of lower porosity (11 μL Å^{-1} g^{-1} in the 10−20 Å region), and day 10 melanin ghosts had a more complex structure (15 μL Å^{-1} g^{-1} at ∼10 Å, with additional porosity up to 50 Å). Melanin from *S. officinalis* ink sacs had a slightly lower peak porosity than the day 4 melanin ghosts (a sharp peak of 29 μL Å^{-1} g^{-1} at 12.5 Å). In contrast, the synthetic tyrosine melanin had the lowest peak porosity (1.1 μL Å^{-1} g^{-1} at 14 Å) (Figure 8A). Additional porosity was distributed in broad peaks in the 300 Å range for all samples (Figure 8A, inset).

With this technique, it is also possible to estimate pore diameter. For all three *C. neoformans* melanin samples, the peak porosity was distributed in pores with diameters ranging from 10 to 20 Å. The day 10 sample also had pores of ∼40 Å. The change in porosity as a function of melanization and time is indicated by the peaks in the pore distribution graph (Figure 8A). This can also be seen from the pore integral graph (Figure 8B). When pore volume was integrated with respect to pore diameter, a rapid increase in the integral was seen in the range of 10−50 Å, corresponding to the presence of pores of that diameter. *S. officinalis* melanin had pores of similar size.

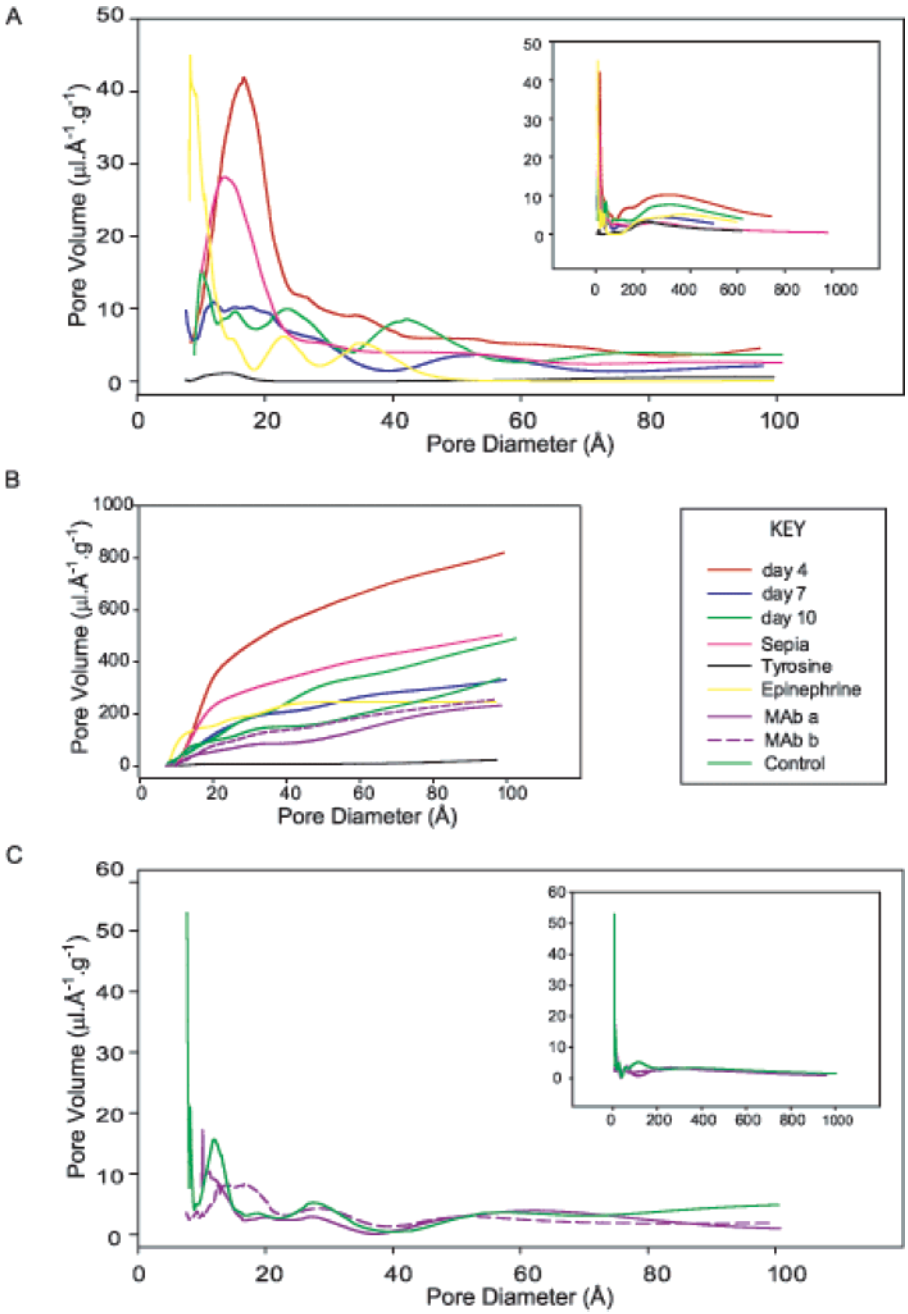

FIGURE 8: NMR cryoporometry of *C. neoformans* melanin ghosts. The color key is beside panel B. (A) Pore distribution graphs for the following melanin samples: *C. neoformans* melanin ghosts isolated from cells grown for 4 (day 4), 7 (day 7), or 10 days (day 10) in the presence of L-dopa, melanin from *S. officinalis* (Sepia), synthetic melanin made from tyrosine (Tyrosine), or *C. neoformans* melanin ghosts made from cells grown for 10 days in the presence of epinephrine (Epinephrine). The inset shows the pore distribution over a larger diameter range. (B) Pore integrals for samples in panel A. Pore volume was integrated with respect to pore diameter. (C) Pore distribution graphs for 10 day L-dopa-derived melanin ghosts incubated with control antibody (control) or melanin-binding antibody (MAb a and b). The results of two experiments are shown for the melanin-binding antibody. The inset shows the pore distribution over a larger diameter range.

The Antibody to Melanin Reduces Porosity. Prior studies showed that addition of melanin-binding antibody to melanized cells arrested cell growth (*9*). We hypothesized that this phenomenon may reflect plugging of melanin pores by specific antibody, a phenomenon that could interfere with cellular nutrition or replicative functions. When melanin ghosts were incubated with a monoclonal antibody against melanin, the total porosity was reduced compared to that with the control antibody. For the control antibody, a peak porosity of ~16 μL Å^{-1} g^{-1} was observed for pores with a diameter of ~12 Å. With the melanin antibody, the porosity was 8 μL Å^{-1} g^{-1} for pores of this diameter (Figure 8C).

Melanins Made from Various Substrates Have Similar Structures. Since *C. neoformans* can synthesize melanin from a variety of substrates, we evaluated the porosity and surface structure of melanin ghosts generated from other substrates. Melanin from *C. neoformans* grown in the presence of epinephrine had a porosity distribution similar to that of melanin made from L-dopa. The pore volume of epinephrine-derived melanin ghosts was distributed in pores ~10 Å in diameter (Figure 8A). To compare the surface structure, *C.*

neoformans strain 24067 was grown in the presence of dopamine for 14 days and melanin ghosts were isolated. ScEM of the isolated ghosts revealed a granular surface for the dopamine ghosts similar to that with L-dopa (Figure 1B). We next examined the surface of melanin ghosts isolated from infected mouse brain tissue. In vivo, *C. neoformans* is thought to use various neurotransmitters from the host as substrates for melanin production (*41*). Ghosts were isolated from mouse brain 21 days after infection by intravenous injection with 5×10^5 *C. neoformans* cells. ScEM analysis of ghosts recovered from mouse tissue revealed a granular surface similar to that of cells grown in vitro (compare panels B and C of Figure 1).

DISCUSSION

Determining the structure of melanin in the *C. neoformans* cell wall is essential to understanding the function of melanin with regard to both cell growth and virulence. Previous studies found that melanin can protect fungal cells against insults that this organism is likely to encounter in both the environment and animal hosts. How melanin affects the structure and function of the fungal cell is a fundamental question in the biology of *C. neoformans* and other fungi that melanize their cell wall. In this study, we applied multiple techniques to address the problem of melanin structure: AFM and ScEM to examine the surface structure of melanin, TEM to study melanin in cross section, and NMR cryoporometry to analyze the porosity of melanin. The results are internally consistent and provide information for modeling the structure of the melanized cell wall and the budding process in melanized cells. Furthermore, these results may serve as a basis for future investigations into the cellular structures of diverse melanized microbes.

The AFM and ScEM images revealed that the surface of melanin ghosts derived from melanized *C. neoformans* cells is composed of discrete granules with roughly uniform dimensions. Depending on the imaging technique that was used, the melanin particles ranged in size from 40 to >100 nm with the average particle diameter being 76 ± 23 nm based on all measurements using both ScEM and AFM. A significant difference was found for granule size measured by ScEM versus AFM for 3 week melanin ghosts. The larger measurements for ScEM may be explained by the fact that samples are coated with 10−15 nm of gold−palladium prior to viewing in the EM, or by the intrinsic magnification error of the microscope (5%). Alternatively, the differences may be due to the fact that the measurements were made from a small number of melanin ghosts, and may reflect natural variation in granule size.

The observation that melanin ghosts from melanized *C. neoformans* are composed of assemblies of smaller melanin particles is consistent with published reports on the structure of melanin from other biological sources. Melanin produced in the ink sacs of the cuttlefish *S. officinalis* consisted of particles 150 nm in diameter by AFM imaging (*42*). Other studies using high-resolution ScEM and TEM methods showed that melanin from *S. officinalis* and bovine eye was comprised of aggregates of smaller particles approximately 20 nm in diameter (*43*, *44*). Melanin granules have also been reported in other fungi. Scytalone-derived melanin in *Verticillium dahliae* formed 100 nm granules in the cell wall when observed by ScEM and TEM (*45*). In *Histoplasma capsulatum*, L-dopa-derived granules have been reported (*46*). Hence, the structure of melanin in *C. neoformans* ghosts and in other biological sources may be similar and composed of small particles that differ in their three-dimensional organization.

Sections of melanin ghosts were analyzed by TEM, revealing that the melanin ghosts are composed of two to five layers arranged in a concentric manner to form the melanin ghost wall. When melanin ghosts from budding cells were examined by TEM, the melanin around the bud was thinner than that of the mother cell. As bud size increased relative to the mother cell, the melanin also appeared to increase in thickness. Together, these data are consistent with an increase in melanin thickness with age, possibly by the addition of more layers of similar-sized particles. Furthermore, the TEM images of melanin ghosts from budding cells support the hypothesis that melanin is degraded or remodeled in budding of *C. neoformans*. This is particularly apparent from the image of the smallest bud in which it appears that a break has been made in the melanin, allowing the bud to emerge (Figure 7A).

On the basis of the microscopy results, we propose that melanin in the *C. neoformans* cell wall is composed of one or more layers of closely packed granules. This is supported by the observation that the surfaces of the melanin ghosts were covered with granular particles ~75 nm in diameter, and by the fact that discrete layers that can be viewed by TEM were approximately the same width of one granule diameter. A question raised by this model is how the melanin granules are held together. One possibility is that they are simply cross-linked together. Alternatively, they could be held together by a lattice or scaffold composed of melanin and/or proteins and polysaccharides. The existence of such a scaffold would have implications for growth and budding of melanized *C. neoformans*, since remodeling of melanin during the budding process could be achieved by degradation of the scaffold. Furthermore, it implies the existence of enzymes required for building and degrading the scaffold. The melanin layers observed in melanin ghosts are reminiscent of cell wall layers observed for *C. neoformans* cells (*47*, *48*). Multilaminate structures are a general feature of fungal cell walls (*49*). Thus, there exist structures in the fungal cell wall that could serve to direct the deposition of melanin into layers.

Since melanized cells continue to replicate and do not show an obvious growth defect relative to nonmelanized cells (*22*), we surmised that they must have pores for nutrient acquisition. However, no large pores were visible by microscopy. One possibility is that, rather than having conventional pores, nutrients and other molecules pass through the melanin layer by diffusing through the spaces between the granules. NMR cryoporometry was utilized to determine the porosity of melanin ghosts from *C. neoformans*. NMR cryoporometry revealed that melanin ghosts had pores and that their porosity decreased with the increasing age of the culture from which the ghosts were generated. This may reflect increased synthesis of melanin and/or cross-linking with time. In addition, the studies revealed a complex pore distribution. Most of the pore volume was distributed in relatively small pores 10−20 Å in diameter. However, some pore volume was also distributed in larger pores 300 Å in diameter.

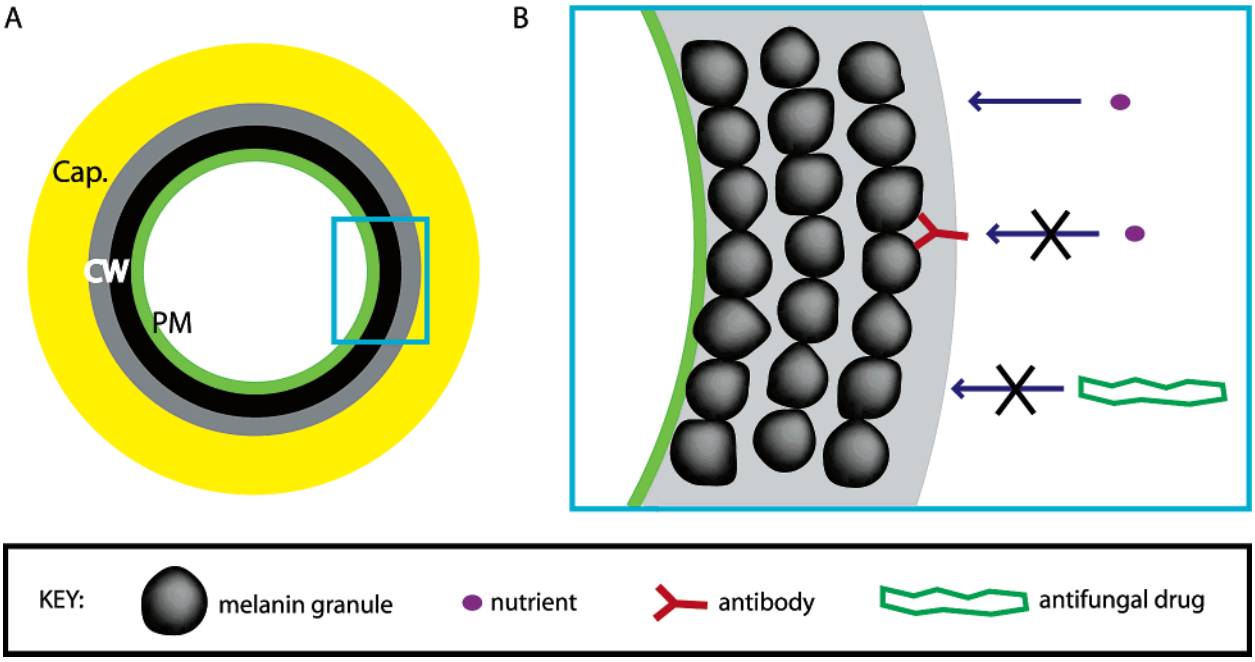

FIGURE 9: Model of melanin structure in *C. neoformans*. (A) Cross-sectional depiction of the *C. neoformans* cell. The polysaccharide capsule (Cap.) surrounds the cell. Melanin (black) is localized to the cell wall (CW), next to the plasma membrane (PM). (B) Cross-sectional depiction of melanin microstructure in the cell wall of *C. neoformans*. The melanin is comprised of multiple layers of granular particles. According to the model, small nutrient molecules, such as sugars and amino acids, can enter the cell by passing through spaces between the melanin particles. Antibody binding to melanin may prevent passage of nutrients by blocking such spaces. In addition, the large size of certain antifungal drugs may prevent their passage through the tight spaces between melanin granules.

Antibody studies provided additional insights into melanin porosity. Melanin ghosts were incubated with melanin-binding antibodies prior to performance of the NMR cryoporometry analysis, and we found a reduction in the measured pore volume of melanin, for pores less than 20 Å in diameter. The most straightforward explanation for this phenomenon is that the antibody binds to the melanin granules and blocks the pore by physical occupation. In contrast, the melanin-binding antibody had no effect on pore volume of pores 300 Å in diameter, suggesting that these pores were inaccessible to the antibody (Figure 8C, inset). Together, these results suggest that melanin ghosts have two sets of pores: (1) smaller, external pores accessible to antibody and (2) larger internal pores inaccessible to antibody.

The NMR cryoporometry results have implications for the arrangement of melanin granules, which approximate microspheres. The predicted volume for a closely packed hexagonal array of spheres is approximately one-fifth the size of the sphere, 15 nm in this case (*37*). Therefore, the NMR cryoporometry results imply that the granules in melanin ghosts are of an irregular shape and arrangement.

Therefore, we propose a model of melanin structure and function in which irregularly shaped melanin granules are fused in layers (Figure 9). The spaces between granules are represented by the small pores observed with NMR cryoporometry. In contrast, the internal spaces between layers are larger, represented by the larger-sized pores. Such a structure enables the melanin to act as a "sieve", allowing certain molecules to pass through, but restricting the passage of larger molecules into the cell. This function is augmented by the fact that melanin also binds and sequesters many such molecules (*50*). The ability of melanin to bind various molecules can be explained by the highly charged and aromatic melanin surface (*11*, *51*).

This model implies that melanin porosity is a property of the arrangement of melanin particles, and consequently, there appears to be no need for specialized pore structures to permit nutrient acquisition. The measured pore size of 10−20 Å is similar to the size of glucose and amino acid molecules. Larger molecules, such as amphotericin B, which has been found to form large aggregates, might be too large to fit in the pores (*52*). Hence, the resistance of melanized cells to amphotericin B may reflect inability of this drug to penetrate the cell wall. The measured and predicted pore sizes suggest a theoretical limit to the size of antifungal drugs which can be expected to be effective against melanotic fungi.

Prior studies have shown that addition of melanin-binding antibodies to melanized *C. neoformans* cells arrests their growth but has no effect on nonmelanized cells (*9*). Since nutrition is essential for growth and nutrient acquisition by melanized cells would almost certainly require competent pores, the ability of a specific antibody to reduce pore size could account for the observed growth arrest. Pore blocking by a specific antibody resulting in a starvation state would represent a novel protective function for antibody-mediated inhibition of *C. neoformans*.

NMR cryoporometry has been used to study cross-linking in polymer systems (*53*). There have also been a number of studies of pore sizes in zeolite skeletons. A caveat of the NMR cryoporometry results is that the melanin ghost preparation may affect the porosity of melanin from *C. neoformans*. However, this application of NMR cryoporometry to the study of pores in melanin shells of fungi is a novel application of this technique to the biological world. These melanin ghosts offer a clean system for NMR

cryoporometry, as there are no changes to the bulk melting point caused by dissolved components in the water. All changes to the melting point arise from the Gibbs−Thomson dimensional effects on the thermodynamics of the system. However, given that the technique of cryoporometry does not require desiccation of the sample, there is now a clear interest in investigating the extent to which it can be applied to the study of other, nonmelanized biological systems. This study has shown that NMR cryoporometry has the necessary sensitivity for measuring the size and volume of pores in biological polymers, and thus potentially is a technique with a large number of new applications in the biological field.

REFERENCES

1. Perfect, J. R., and Casadevall, A. (2002) Cryptococcosis, *Infect. Dis. Clin. North Am. 16*, 837−874, v−vi.
2. Buchanan, K. L., and Murphy, J. W. (1998) What makes *Cryptococcus neoformans* a pathogen? *Emerg. Infect. Dis. 4*, 71−83.
3. Hull, C. M., and Heitman, J. (2002) Genetics of *Cryptococcus neoformans*, *Annu. Rev. Genet. 36*, 557−615.
4. Casadevall, A., Rosas, A. L., and Nosanchuk, J. D. (2000) Melanin and virulence in *Cryptococcus neoformans*, *Curr. Opin. Microbiol. 3*, 354−358.
5. Nosanchuk, J. D., and Casadevall, A. (2003) The contribution of melanin to microbial pathogenesis, *Cell. Microbiol. 5*, 203−223.
6. Kwon-Chung, K. J., Polacheck, I., and Popkin, T. J. (1982) Melanin-lacking mutants of *Cryptococcus neoformans* and their virulence for mice, *J. Bacteriol. 150*, 1414−1421.
7. Salas, S. D., Bennett, J. E., Kwon-Chung, K. J., Perfect, J. R., and Williamson, P. R. (1996) Effect of the laccase gene CNLAC1, on virulence of *Cryptococcus neoformans*, *J. Exp. Med. 184*, 377−386.
8. Alviano, D. S., Franzen, A. J., Travassos, L. R., Holandino, C., Rozental, S., Ejzemberg, R., Alviano, C. S., and Rodrigues, M. L. (2004) Melanin from *Fonsecaea pedrosoi* induces production of human antifungal antibodies and enhances the antimicrobial efficacy of phagocytes, *Infect. Immun. 72*, 229−237.
9. Rosas, A. L., Nosanchuk, J. D., and Casadevall, A. (2001) Passive immunization with melanin-binding monoclonal antibodies prolongs survival of mice with lethal *Cryptococcus neoformans* infection, *Infect. Immun. 69*, 3410−3412.
10. Nosanchuk, J. D., Rosas, A. L., and Casadevall, A. (1998) The antibody response to fungal melanin in mice, *J. Immunol. 160*, 6026−6031.
11. Nosanchuk, J. D., Valadon, P., Feldmesser, M., and Casadevall, A. (1999) Melanization of *Cryptococcus neoformans* in murine infection, *Mol. Cell. Biol. 19*, 745−750.
12. Huffnagle, G. B., Chen, G. H., Curtis, J. L., McDonald, R. A., Strieter, R. M., and Toews, G. B. (1995) Down-regulation of the afferent phase of T cell-mediated pulmonary inflammation and immunity by a high melanin-producing strain of *Cryptococcus neoformans*, *J. Immunol. 155*, 3507−3516.
13. Mohagheghpour, N., Waleh, N., Garger, S. J., Dousman, L., Grill, L. K., and Tuse, D. (2000) Synthetic melanin suppresses production of proinflammatory cytokines, *Cell. Immunol. 199*, 25−36.
14. Wang, Y., Aisen, P., and Casadevall, A. (1995) *Cryptococcus neoformans* melanin and virulence: Mechanism of action, *Infect. Immun. 63*, 3131−3136.
15. Doering, T. L., Nosanchuk, J. D., Roberts, W. K., and Casadevall, A. (1999) Melanin as a potential cryptococcal defence against microbicidal proteins, *Med. Mycol. 37*, 175−181.
16. Ikeda, R., Sugita, T., Jacobson, E. S., and Shinoda, T. (2003) Effects of melanin upon susceptibility of *Cryptococcus* to antifungals, *Microbiol. Immunol. 47*, 271−277.
17. van Duin, D., Casadevall, A., and Nosanchuk, J. D. (2002) Melanization of *Cryptococcus neoformans* and *Histoplasma capsulatum* reduces their susceptibilities to amphotericin B and caspofungin, *Antimicrob. Agents Chemother. 46*, 3394−3400.
18. Wang, Y., and Casadevall, A. (1994) Growth of *Cryptococcus neoformans* in the presence of L-dopa decreases its susceptibility to amphotericin B, *Antimicrob. Agents Chemother. 38*, 2648−2650.
19. Nosanchuk, J. D., Rudolph, J., Rosas, A. L., and Casadevall, A. (1999) Evidence that *Cryptococcus neoformans* is melanized in pigeon excreta: Implications for pathogenesis, *Infect. Immun. 67*, 5477−5479.
20. Wang, Y., and Casadevall, A. (1994) Susceptibility of melanized and nonmelanized *Cryptococcus neoformans* to nitrogen- and oxygen-derived oxidants, *Infect. Immun. 62*, 3004−3007.
21. Garcia-Rivera, J., and Casadevall, A. (2001) Melanization of *Cryptococcus neoformans* reduces its susceptibility to the antimicrobial effects of silver nitrate, *Med. Mycol. 39*, 353−357.
22. Rosas, A. L., and Casadevall, A. (1997) Melanization affects susceptibility of *Cryptococcus neoformans* to heat and cold, *FEMS Microbiol. Lett. 153*, 265−272.
23. Wang, Y., and Casadevall, A. (1994) Decreased susceptibility of melanized *Cryptococcus neoformans* to UV light, *Appl. Environ. Microbiol. 60*, 3864−3866.
24. Mylonakis, E., Ausubel, F. M., Perfect, J. R., Heitman, J., and Calderwood, S. B. (2002) Killing of *Caenorhabditis elegans* by *Cryptococcus neoformans* as a model of yeast pathogenesis, *Proc. Natl. Acad. Sci. U.S.A. 99*, 15675−15680.
25. Steenbergen, J. N., Shuman, H. A., and Casadevall, A. (2001) *Cryptococcus neoformans* interactions with amoebae suggest an explanation for its virulence and intracellular pathogenic strategy in macrophages, *Proc. Natl. Acad. Sci. U.S.A. 98*, 15245−15250.
26. Nosanchuk, J. D., and Casadevall, A. (2003) Budding of melanized *Cryptococcus neoformans* in the presence or absence of L-dopa, *Microbiology 149*, 1945−1951.
27. Polacheck, I., Hearing, V. J., and Kwon-Chung, K. J. (1982) Biochemical studies of phenoloxidase and utilization of catecholamines in *Cryptococcus neoformans*, *J. Bacteriol. 150*, 1212−1220.
28. Williamson, P. R. (1994) Biochemical and molecular characterization of the diphenol oxidase of *Cryptococcus neoformans*: Identification as a laccase, *J. Bacteriol. 176*, 656−664.
29. Butler, M. J., and Day, A. W. (1998) Fungal melanins: A review, *Can. J. Microbiol. 44*, 1115−1136.
30. Langfelder, K., Streibel, M., Jahn, B., Haase, G., and Brakhage, A. A. (2003) Biosynthesis of fungal melanins and their importance for human pathogenic fungi, *Fungal Genet. Biol. 38*, 143−158.
31. Wang, Y., Aisen, P., and Casadevall, A. (1996) Melanin, melanin "ghosts," and melanin composition in *Cryptococcus neoformans*, *Infect. Immun. 64*, 2420−2424.
32. Chang, Y. C., and Kwon-Chung, K. J. (1994) Complementation of a capsule-deficient mutation of *Cryptococcus neoformans* restores its virulence, *Mol. Cell. Biol. 14*, 4912−4919.
33. Rosas, A. L., Nosanchuk, J. D., Feldmesser, M., Cox, G. M., McDade, H. C., and Casadevall, A. (2000) Synthesis of polymerized melanin by *Cryptococcus neoformans* in infected rodents, *Infect. Immun. 68*, 2845−2853.
34. Glatman-Freedman, A., Martin, J. M., Riska, P. F., Bloom, B. R., and Casadevall, A. (1996) Monoclonal antibodies to surface antigens of *Mycobacterium tuberculosis* and their use in a modified enzyme-linked immunosorbant spot assay for detection of mycobacteria, *J. Clin. Microbiol. 34*, 2795−2802.
35. Rosas, A. L., Nosanchuk, J. D., Gomez, B. L., Edens, W. A., Henson, J. M., and Casadevall, A. (2000) Isolation and serological analyses of fungal melanins, *J. Immunol. Methods 244*, 69−80.
36. Jackson, C. L., and McKenna, G. B. (1990) The melting behavior of organic materials confined in porous solids, *J. Chem. Phys. 93*, 9002−9011.
37. Webber, J. B. W. (2000) Characterising Porous Media, Ph.D. Thesis, Appendix H, pp 261−263, University of Kent, Canterbury, Kent, U.K.
38. Webber, J. B. W., Strange, J. H., and Dore, J. C. (2001) An evaluation of NMR cryoporometry, density measurement and neutron scattering methods of pore characterization, *Magn. Reson. Imaging 19*, 395−399.
39. Camesano, T. A., and Logan, B. E. (2000) Probing Bacterial Electrostatic Interactions Using Atomic Force Microscopy, *Environ. Sci. Technol. 34*, 3354−3362.
40. Burnham, N. A., Chen, X., Hodges, C. S., Matei, G. A., Thoreson, E. K., Roberts, C. J., Davies, M. C., and Tendler, S. J. B. (2003) Comparison of calibration methods for atomic-force microscopy cantilevers, *Nanotechnology 14*, 1−6.
41. Nosanchuk, J. D., Rosas, A. L., Lee, S. C., and Casadevall, A. (2000) Melanisation of *Cryptococcus neoformans* in human brain tissue, *Lancet 355*, 2049−2050.

42. Clancy, C. M., and Simon, J. D. (2001) Ultrastructural organization of eumelanin from *Sepia officinalis* measured by atomic force microscopy, *Biochemistry 40*, 13353−13360.
43. Liu, Y., and Simon, J. D. (2003) The effect of preparation procedures on the morphology of melanin from the ink sac of *Sepia officinalis*, *Pigm. Cell Res. 16*, 72−80.
44. Clancy, C. M., Nofsinger, J. B., Hanks, R. K., and Simon, J. D. (2000) A hierarchical self-assembly of eumelanin, *J. Phys. Chem. B 104*, 7871−7873.
45. Wheeler, M. H., Tolmsoff, W. J., and Meola, S. (1976) Ultrastructure of melanin formation in *Verticillium dahliae* with (+)-scytalone as a biosynthetic intermediate. *Can. J. Microbiol. 22*, 702−711.
46. Nosanchuk, J. D., Gomez, B. L., Youngchim, S., Diez, S., Aisen, P. Zancope-Oliveira, R. M., Restrepo, A., Casadevall, A., and Hamilton, A. J. (2002) *Histoplasma capsulatum* synthesizes melanin-like pigments in vitro and during mammalian infection. *Infect. Immun. 70*, 5124−5131.
47. al-Doory, Y. (1971) The ultrastructure of *Cryptococcus neoformans*, *Sabouraudia 9*, 115−118.
48. Stoetzner, H., and Kemmer, C. (1971) The morphology of *Cryptococcus neoformans* in human cryptococcosis. A light-, phase-contrast and electron-microscopic study, *Mycopathol. Mycol. Appl. 45*, 327−335.
49. Aronson, J. M. (1965) The Cell Wall, in *The Fungal Cell* (Ainsworth, G. C., and Sussman, A. S., Eds.) pp 49−76, Academic Press, New York.
50. Hill, H. Z. (1992) The function of melanin or six blind people examine an elephant, *BioEssays 14*, 49−56.
51. Nosanchuk, J. D., and Casadevall, A. (1997) Cellular charge of *Cryptococcus neoformans*: Contributions from the capsular polysaccharide, melanin, and monoclonal antibody binding, *Infect. Immun. 65*, 1836−1841.
52. Lamy-Freund, M. T., Schreier, S., Peitzsch, R. M., and Reed, W. F. (1991) Characterization and time dependence of amphotericin B: Deoxycholate aggregation by quasielastic light scattering, *J. Pharm. Sci. 80*, 262−266.
53. Baba, M., Nedelec, J.-M., Lacoste, J., and Gardette, J.-L. (2003) Calibration of cyclohexane solid−solid−phase transition thermoporosimetry and application to the study of cross-linking of elastomers upon aging, *J. Non-Cryst. Solids 315*, 228−238.

BI047731M